Component-Adaptive Grid Embedding

E. H. Atta
Lockheed-Georgia Company

Introduction:

One of the major problems related to transonic flow prediction about realistic aircraft configuration is the generation of a suitable grid which encompasses such configurations. In general, each aircraft component (wing, fuselage, nacelle) requires a grid system that is usually incompatible with the grid systems of the other components; thus, the implementation of finite-difference methods for such geometrically-complex configurations is a difficult task.

In this presentation a new approach is developed to treat such a problem. The basic idea is to generate different grid systems, each suited for a particular component. Thus, the flow field domain is divided into overlapping subdomains of different topology. These grid systems are then interfaced with each other in such a way that stability, convergence speed and accuracy are maintained.

Model:

To evaluate the feasibility of the present approach a two-dimensional model is considered (figure 1). The model consists of a single airfoil embedded in rectangular boundaries, representing an airfoil in a wind tunnel or in free air. The flow field domain is divided into two overlapping subdomains, each covering only a part of the whole field. The inner subdomain employs a surface-fitted curvilinear grid generated by an elliptic grid-generator (ref. 1), while the outer subdomain employs a cartesian grid. The overlap region between the two subdomains is bounded by the outer boundary of the curvilinear grid and the inner boundary of the cartesian grid.

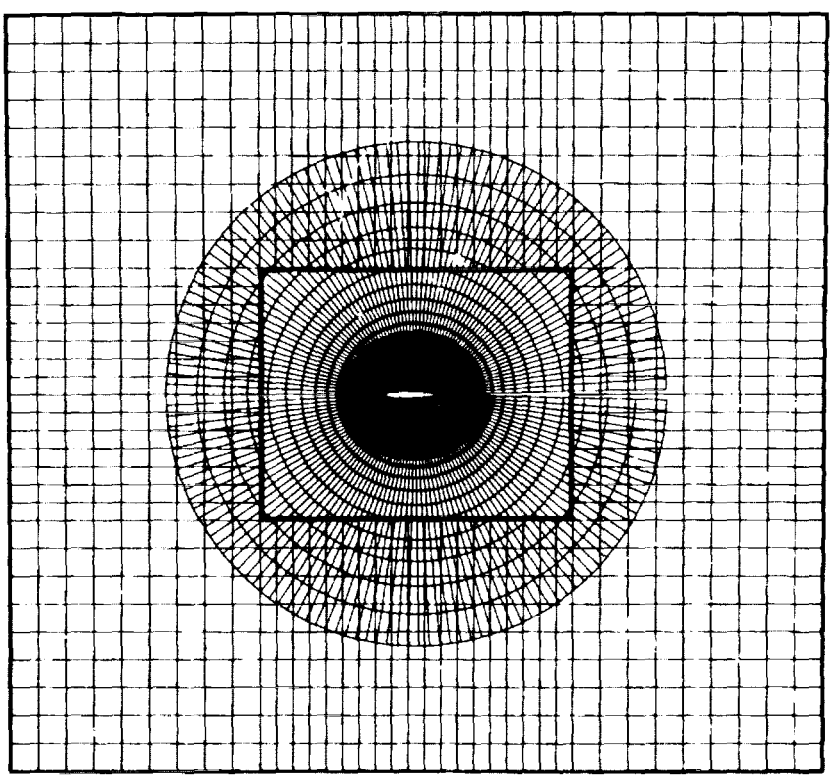

Figure 1.- Composite grid for an airfoil.

Approach:

Figure 2 shows the two subdomains (A,B) of the flow field; each has a grid adapted to suit its geometry. The flow in both subdomains is governed by the transonic full-potential equation. While a Neumann-type boundary condition is used at the inner boundary of subdomain B (overlap inner boundary), a Dirichlet-type boundary condition is used at the outer boundary of subdomain A (overlap outer boundary). These boundary conditions are updated during the solution process. The implicit approximate factorization scheme is used in both grid systems. The code of ref. 1 is modified to fit into the present scheme.

The solution process is performed in cycles, starting by solving for the flow field in subdomain A, then switching after a number of iterations to solve for the flow field in subdomain B. During each cycle the overlap boundary conditions are updated by using a two dimensional second order Lagrangian interpolation scheme. This process is then repeated until convergence is achieved in both subdomains.

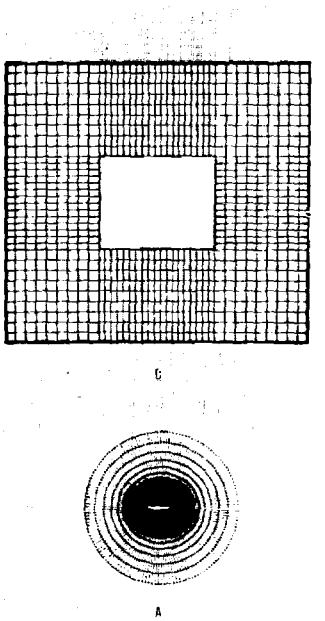

Figure 2.- Grid topology for the different subdomains.

Comparison with a homogeneous grid:

The results of the present method are compared with the results obtained from using one homogeneous grid for the entire flow field (ref. 1). In all the test cases considered, a standard grid with (31 x 147) points and a circular outer boundary located 6 chord-lengths away from the airfoil are used. (See figure 3.)

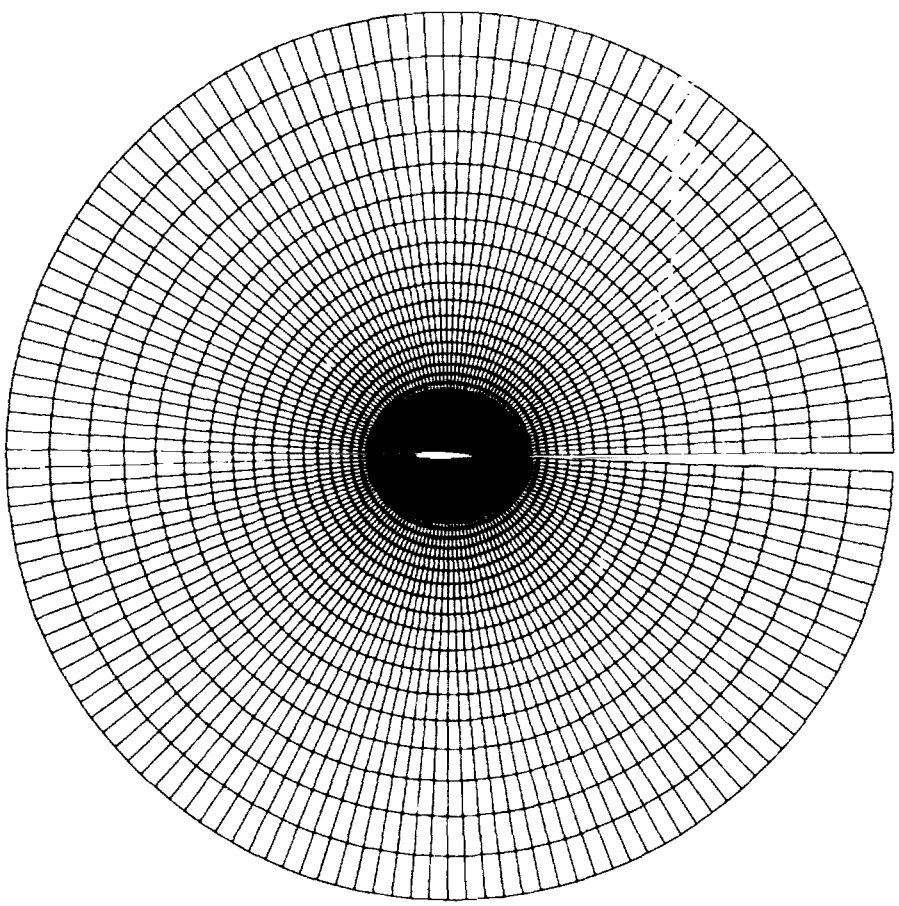

Figure 3.- Uniform grid for an airfoil (ref. 1).

Computed Results:

Results of the present method are compared with the results obtained from the code of ref. 1. Two sets of parameters affecting the performance of the numerical scheme are listed in tables I and II. Figures 4 and 5 display the pressure-coefficient distributions for a NASA-0012 airfoil resulting from the flow field solutions. The results are in good agreement for both subcritical and supercritical cases; savings in computing time are achieved by reducing the size of the flow field covered by the curvilinear grid (subdomain A).

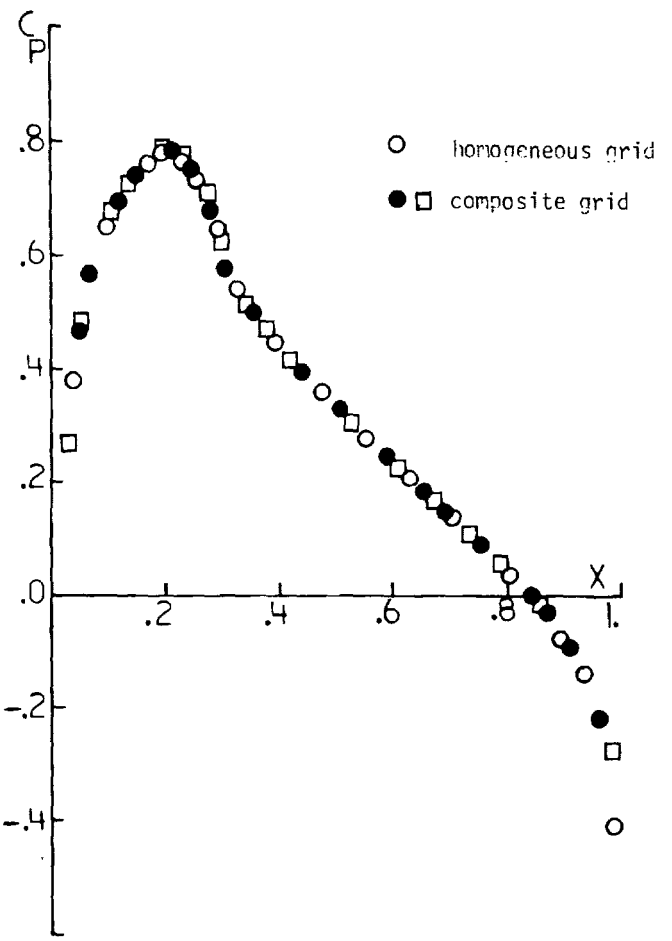

Figure 4.- Comparison of pressure coefficient for NACA-0012. (M_∞ = 0.75, α = 0.)

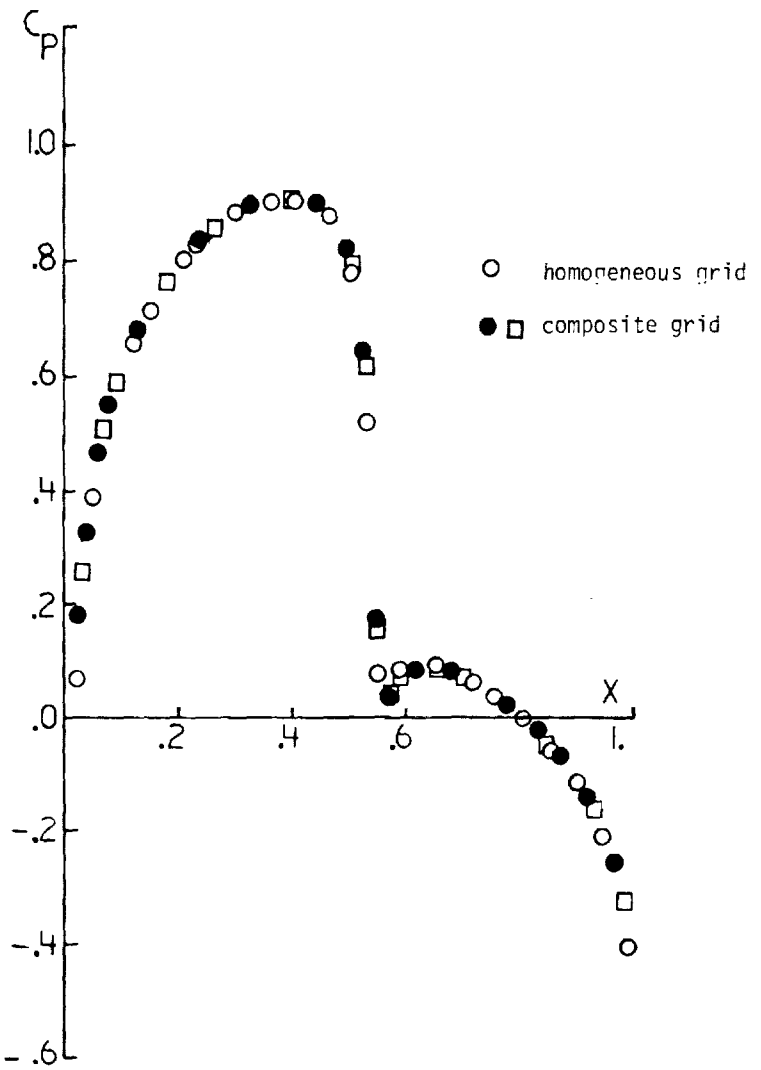

Figure 5.- Comparison of pressure coefficient for NACA-0012.
(M_∞ = 0.8, α = 0.)

Flow Field Topology :

The extent of the overlap region between the different grids and the relative size of each subdomain are the main factors affecting the accuracy and convergence speed of the present scheme. Figure 6 shows the flow field topology for several test cases. In these cases the overlap extent and subdomain sizes are varied to determine their optimum values that will minimize the computing effort, while maintaining a reasonable accuracy.

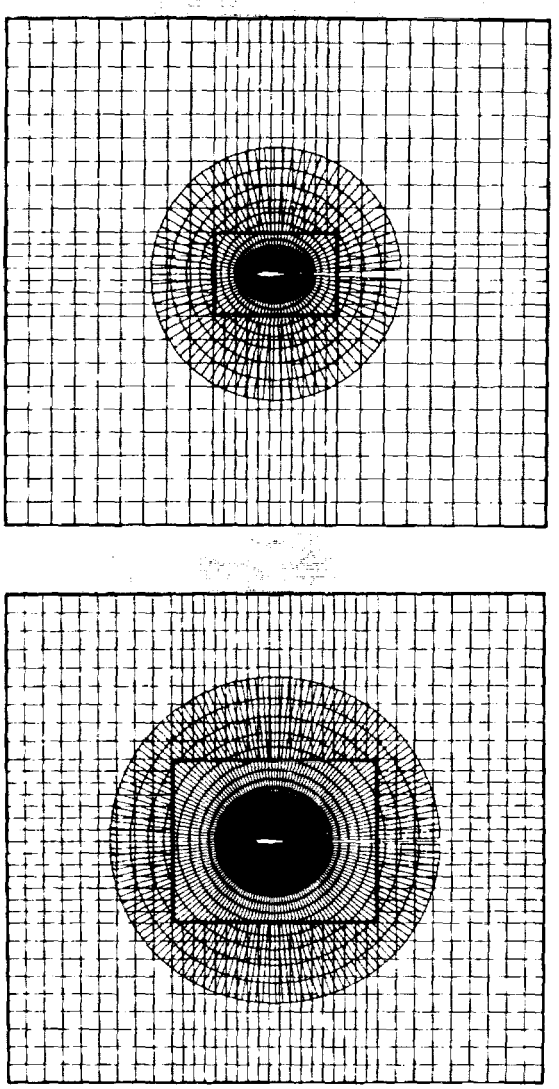

Figure 6.- Flow-field topology with different grid-overlap.

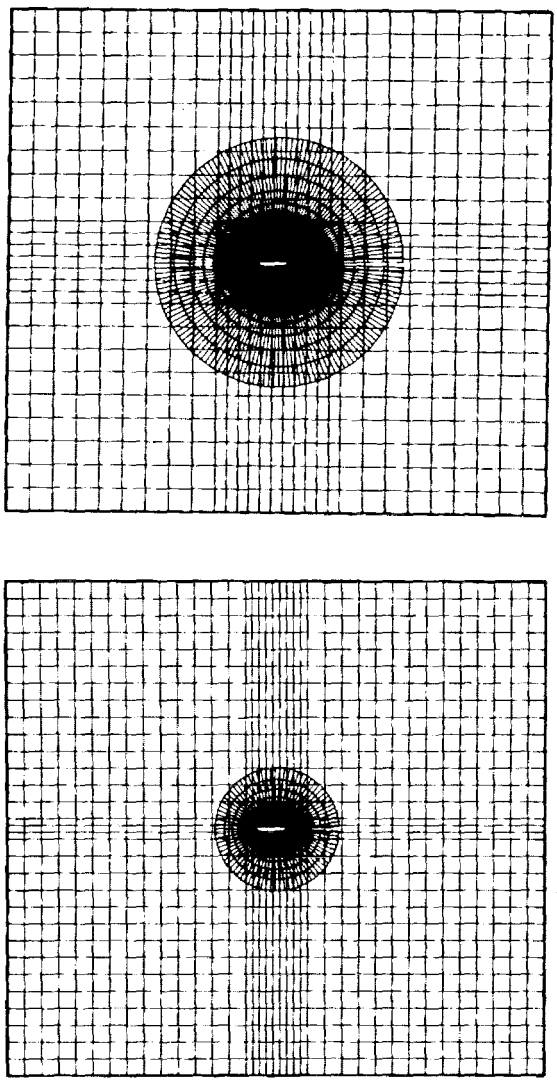

Figure 6.- Concluded.

Overlap arrangement:

Test cases with different grids-arrangement are compared to determine the optimum choice for the extent of the overlap region. A work factor w [number of iterations for convergence x number of grid points (curvilinear grid)] is taken as a measure of the computing effort. Numerical results show that increasing the extent of the overlap region decreases the number of iterations for convergence; however, this also increases the computing effort (figure 7). To minimize the computing time the Cartesian grid should overlap 15-25% of the curvilinear grid, and the inner boundary of the Cartesian grid should not be located less than 0.25 chord-length away from the airfoil.

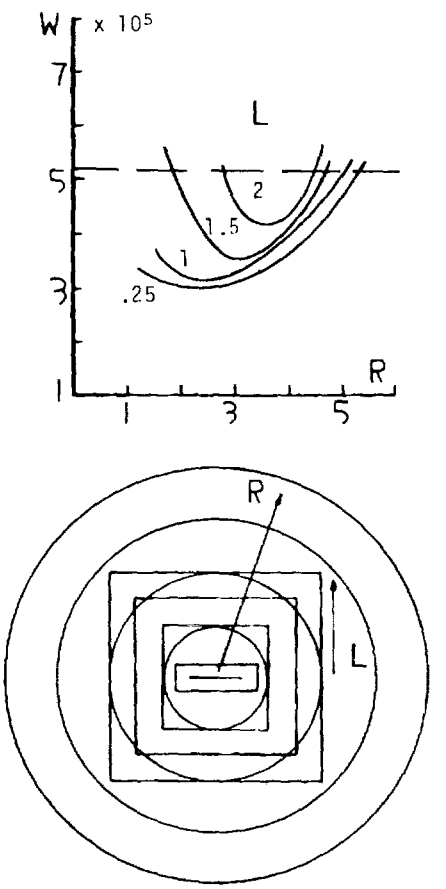

Figure 7.- Effect of overlap parameters on work factor w. (NACA-0012, $M_\infty = 0.8$, $\alpha = 0.$)

Computed Results:

The use of nonoptimal parameters for grids arrangement (overlap extent, relative grid sizes) can produce inaccurate results and/or slow down convergence. The Peaky pressure coefficient distribution shown in figure 8 is corrected by increasing the extent of the overlap region described in Table III.

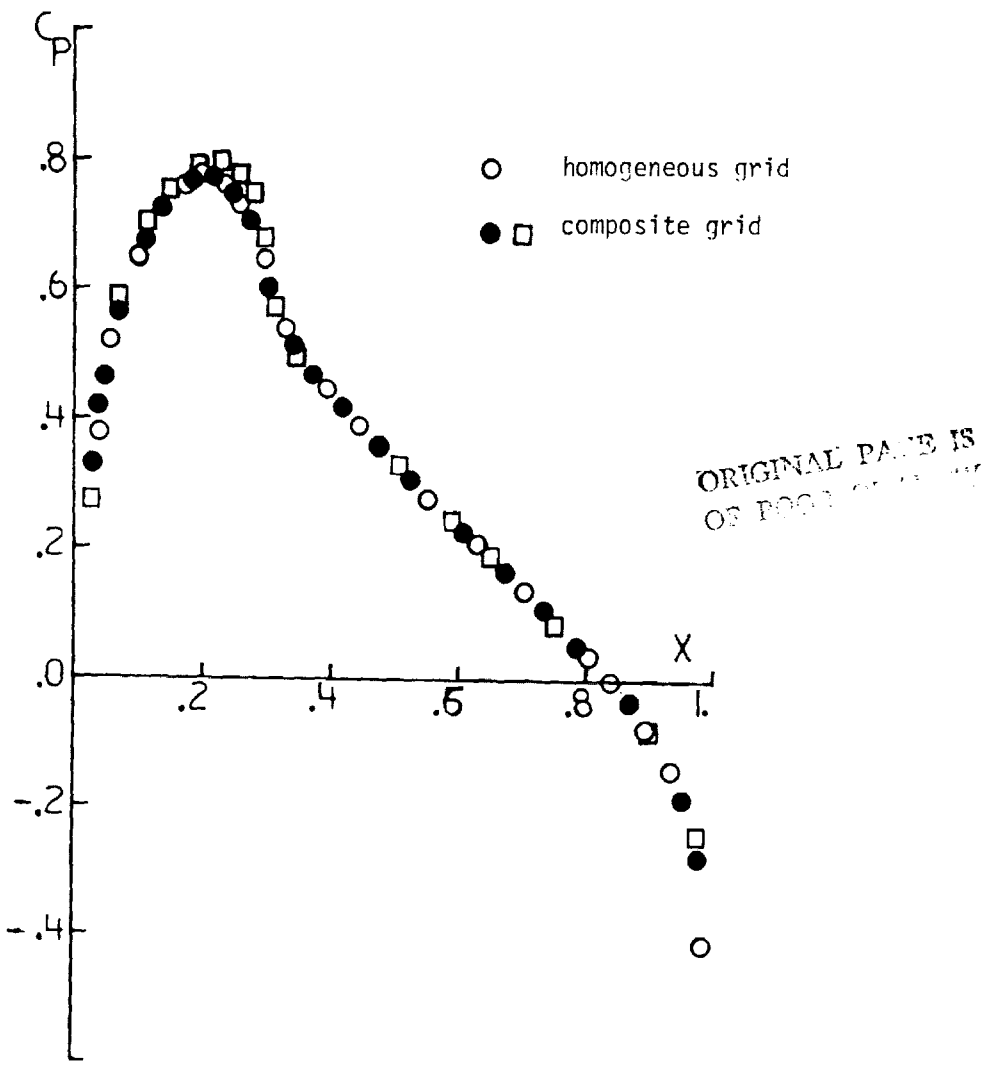

Figure 8.- Comparison of pressure coefficient for NACA-0012. (M_∞ = 0.75, α = 0.)

Computed Results:

Figures 9 and 10 display the pressure coefficient distributions for two lifting cases for the parameters described in Tables IV and V. The evolution of circulation, and hence lift, is slowed down as the solution process alternates between the different grids. This is dealt with by decreasing the number of iterations performed in each grid.

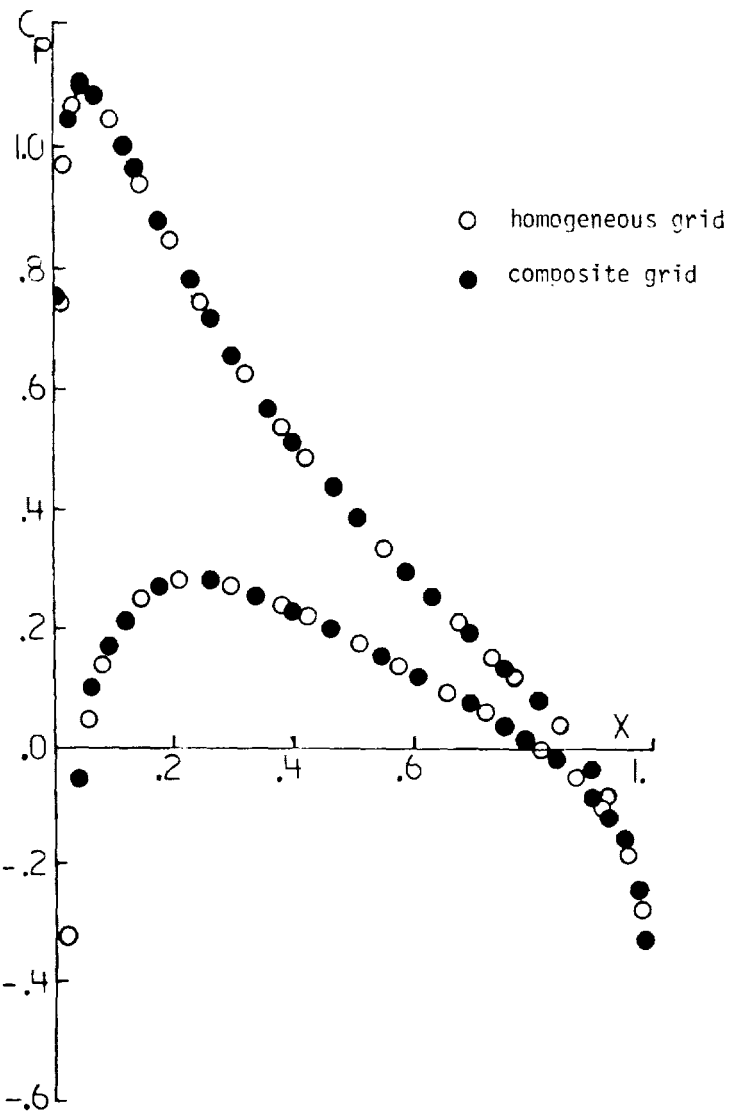

Figure 9.- Comparison of pressure coefficient for NACA-0012. ($M_\infty = 0.63$, $\alpha = 2^o$.)

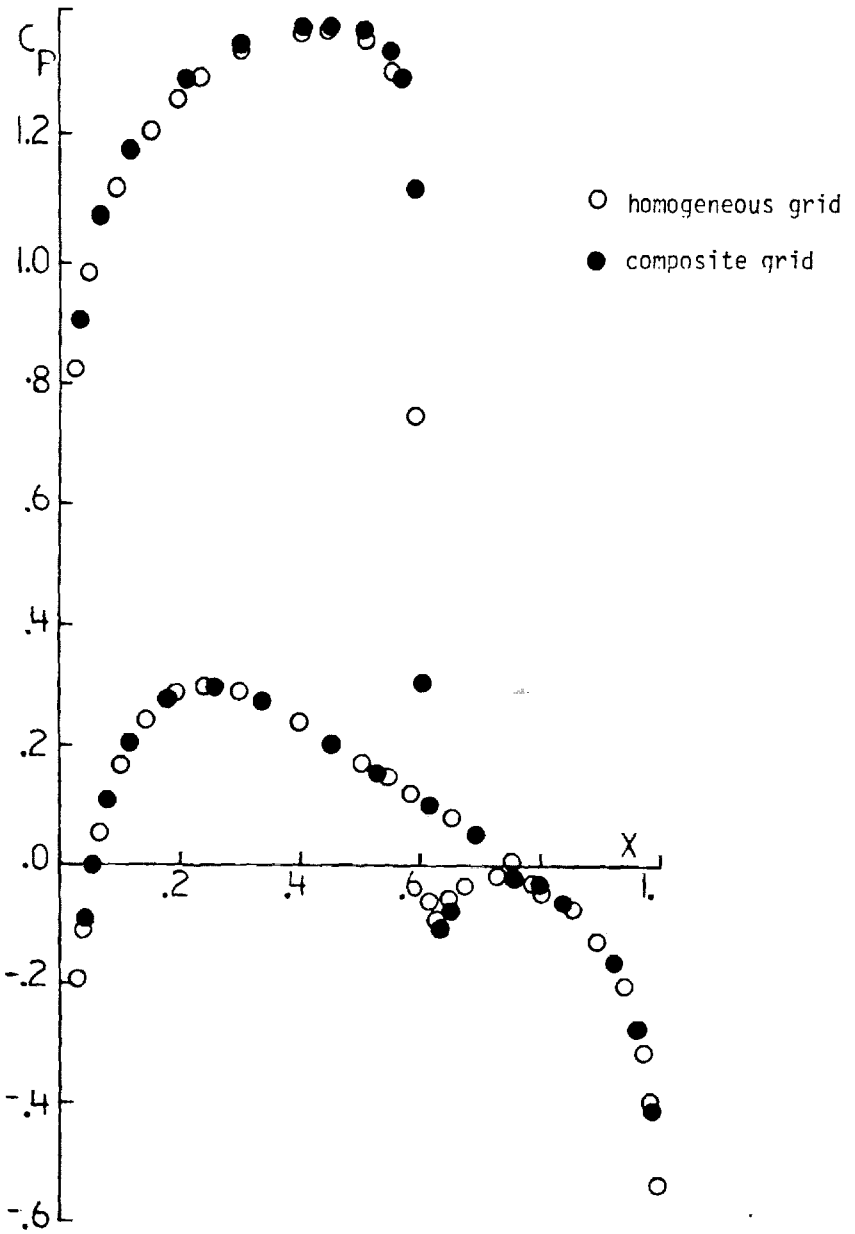

Figure 10.- Comparison of pressure coefficient for NACA-0012.
(M_∞ = 0.75, α = 2°.)

Errors in sonic line position:

Should the shock wave extend into the overlap region, the interpolation process can produce errors in the shock location and strength. Comparisons of the results of the present method with those of a homogeneous grid shows that the maximum relative error did not exceed 1.5%. (See figure 11.)

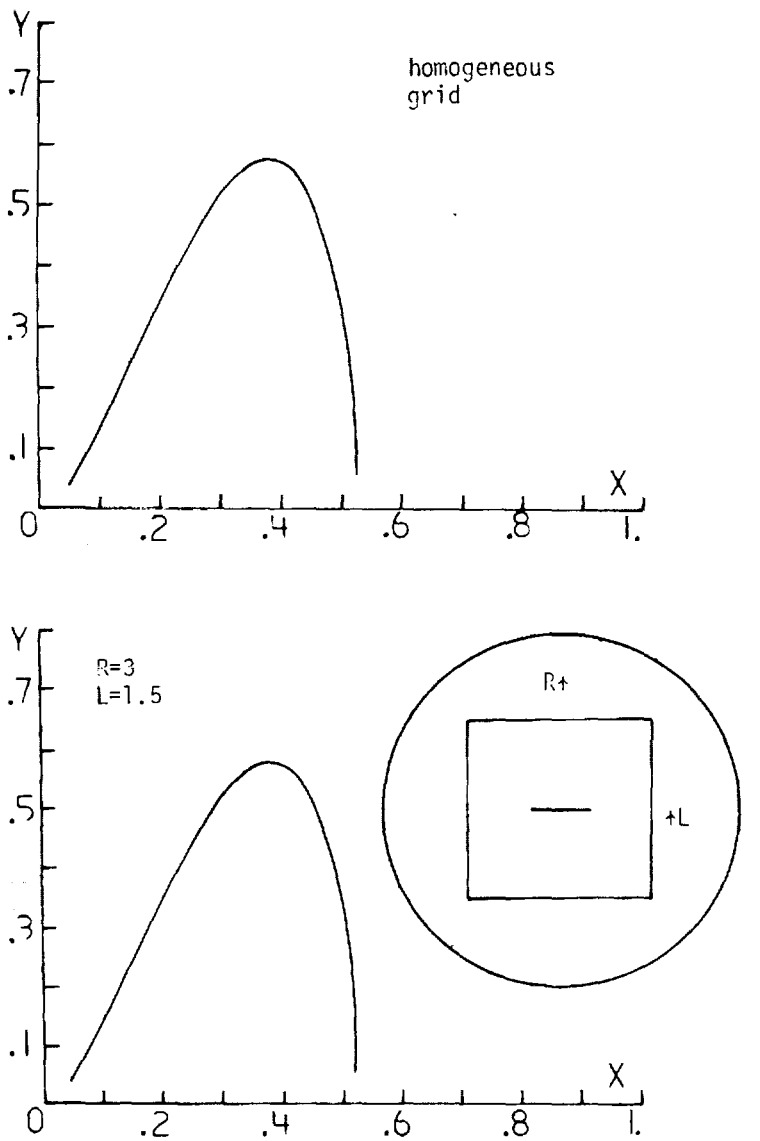

Figure 11.- Effect of interface location on sonic line position. (NACA-0012, $M_\infty = 0.8$, $\alpha = 0.$)

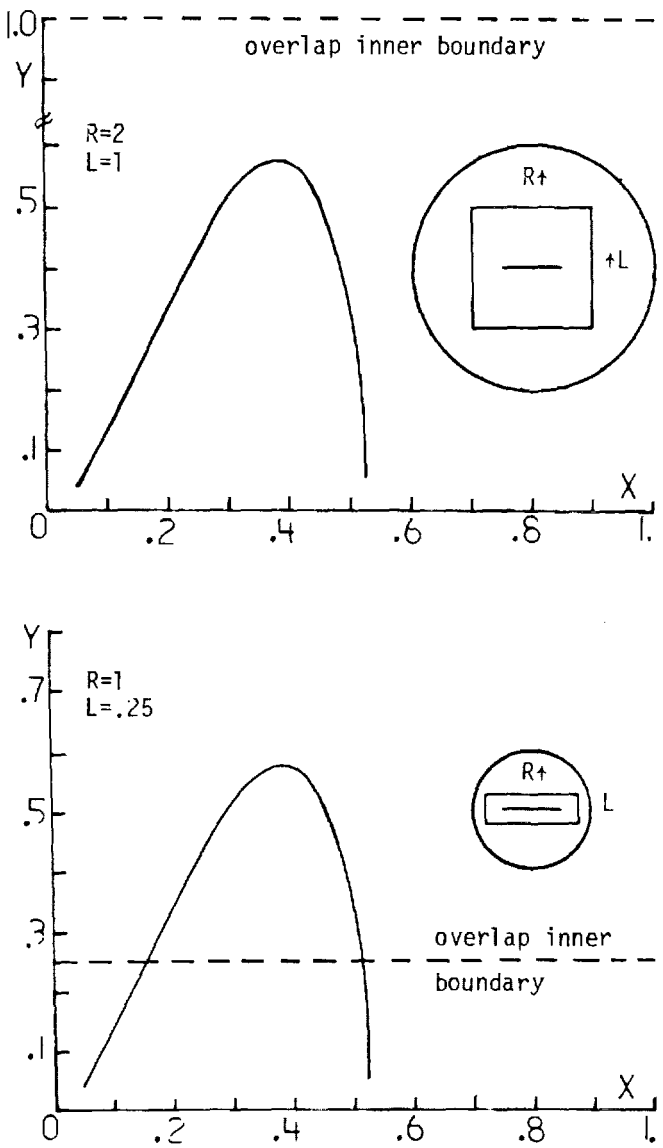

Figure 11.- Concluded.

Conclusion:

A method for interfacing grid systems of different topology is developed. This offers a new approach to the problem of transonic flow prediction about multiple-component configurations. The method is implemented in a 2-D domain containing two grid systems of different topology. The numerical scheme in the present method proved to be stable and accurate. Savings in computer time and/or storage is achieved by the proper choice of the overlap region between the different grids.

Reference:

1. Holst, T. L., "Implicit Algorithm for the Conservative Transonic Full-Potential Equation Using an Arbitrary Mesh," AIAA J., Vol. 17, No. 10, October 1979.

TABLE I

	Code of Ref. 1 TAIR Code	Present Method	
Curvilinear grid	31 x 147	15 x 147	21 x 147
Cartesian grid		30 x 30	30 x 30
% cpu time reduction as compared to TAIR Code		30%	10%
location of subdomain B outer boundary		6 chord-length	6 chord-length
Location of subdomain B inner boundary		1 chord-length	2 chord-length
Location of subdomain A outer boundary		1 chord-length	4 chord-length
number of cycles for convergence		9	10

TABLE II

	Code of Ref. 1 TAIR Code	Present Method	
Curvilinear grid	31 x 147	18 x 147	14 x 147
Cartesian grid		30 x 30	50 x 50
% cpu time reduction as compared to TAIR Code		20%	10%
location of subdomain B outer boundary		6 chord-length	6 chord-length
location of subdomain B inner boundary		1 chord-length	1/4 chord-length
location in subdomain A outer boundary		2 chord-length	1 chord length
number of cycles for convergence		12	15

TABLE III

	Code of Ref. 1 TAIR Code	Present Method	
Curvilinear grid	31 x 147	10 x 147	15 x 147
Cartesian grid		30 x 30	40 x 40
location of subdomain B outer boundary		6 chord-length	6 chord-length
location of subdomain B inner boundary		1/4 chord-length	1/4 chord-length
location of subdomain A outer boundary		1.5 chord-length	1 chord-length

TABLE IV

	Code of Ref. 1 TAIR Code	Present Method
Curvilinear grid	31 x 147	15 x 147
Cartesian grid		30 x 40
% cpu time reduction as compared to TAIR Code		39%
location of subdomain B outer boundary		6 chord-length
location of subdomain B inner boundary		1 chord-length
location of subdomain A outer boundary		3 chord-length
lift coefficient	0.334	0.337
number of cycles for convergence		16

TABLE V

	Code of Ref. 1 TAIR Code	Present Method
Curvilinear grid	31 x 147	21 x 147
Cartesian Grid		30 x 30
% cpu time reduction as compared to TAIR Code		2%
location of subdomain B outer boundary		6 chord-length
location of subdomain B inner boundary		2 chord-length
location of subdomain A outer boundary		4 chord-length
lift coefficient	0.574	.584
number of cycles for convergence		14